Available online at www.sciencedirect.com

ScienceDirect

Ceramics International 39 (2013) 9491–9498

CERAMICS INTERNATIONAL

www.elsevier.com/locate/ceramint

Large-scale synthesis of uniform lanthanum oxide nanowires *via* template-free deposition followed by heat-treatment

Fatemeh Khosrow-pour[a], Mustafa Aghazadeh[b,*], Behrouz Sabour[b], Somayeh Dalvand[b]

[a]*Department of Chemistry, Islamic Azad University, Saveh Branch, Saveh, Iran*
[b]*Department of Chemistry, Faculty of Science, Islamic Azad University, Shahr-e-Ray Branch, Tehran, Iran*

Received 17 March 2013; received in revised form 7 April 2013; accepted 16 May 2013
Available online 23 May 2013

Abstract

A simple two-step method is proposed for the large scale preparation of La_2O_3 nanowires without any template and additive: (i) cathodic electrodeposition and (ii) heat-treatment. In the first step, $La(OH)_3$ was easily deposited on the steel cathode from 0.005 M $La(NO_3)_3$ bath by applying I_a of 2 mA cm^{-2}. In the second one, the prepared hydroxide precursor was heat-treated at 600 °C for 3 h in dry air atmosphere. The physico-chemical changes of the hydroxide deposit on heating were investigated by DSC–TG analysis and the results were discussed. The structural characterizations by XRD and FT-IR, and morphological observations *via* SEM revealed that well-crystallized and uniform La_2O_3 nanowires are easily achievable *via* cathodic deposition followed by heat-treatment.

Keywords: A. Calcination; A. Powders; B. Electron microscopy; D. Transistion metal oxides: Electrochemical preparation

1. Introduction

One-dimensional (1D) nano-scale materials have been intensively investigated for their potential applications in numerous scientific fields. Lanthanides are an attractive class of elements and have unique optical, catalytic and magnetic properties as a consequence of their unique 4f electrons configuration. Among various lanthanum-based materials, lanthanum oxide (La_2O_3) is of great research interest due to its technological applications as gate insulator, superconductive, hydrogen storage, electrode and sorbent materials [1–6]. Also, La_2O_3 has received increasing attentions because it is extensively used as piezo-electricity, galvanothermy and thermoelectricity materials, and also as light-emitting phosphors, catalyst support and automobile exhaust-gas convector components [7–15].

In recent years, the preparation of low-dimensional La_2O_3 and $La(OH)_3$ nanostructures has received intensive interest. For example, a variety of nanostructures of La_2O_3 and $La(OH)_3$ such as nanotubes [16,17], nanorods [17–29], nanospindles [29], nanowires [30], nanocapsules [31], nanoplates [25,32], nanospheres [33] and nanobelts [34] have been prepared by various methods. Furthermore, particular attention has been given to the design of easy and facile synthetic routes, which can motivated the preparation of 1D nanostructures of La_2O_3 at large scale with high quality. The applied methods in the preparation of La_2O_3 and $La(OH)_3$ nanostructures can be classified into three type of methods: physical (*e.g.*, atomic layer deposition [35–37]), chemical (*e.g.*, solvothermal [19–21], chemical participation [23,38], hydrothermal [11,22,33,34,39], thermal decomposition [40] and sol–gel [18,41]), and electrochemical (*e.g.*, cathodic electrodeposition [16,17,27–32,42,43]).

Electrochemical synthesis has been mentioned as an easy, effective, flexible and powerful method for the preparation of nanostructured metal oxide and hydroxides [44–48]. This technique considers many parameters such as potential, current density, bath conditions (temperature, concentration, pH and additives), electrode and electrolyte type, which one can manipulate to control the physico-chemical and the morphological properties of the products. In recent years, various 1D nanostructures of $La(OH)_3$ and La_2O_3 have been prepared *via* this route by applying different synthetic conditions [16,17,27–32]. For example, high quality arrays of $La(OH)_3$ and La_2O_3 nanotubes have been fabricated by the cathodic electrodeposition process using anodic alumina membrane templates [16].

*Corresponding author. Tel./fax: +98 21 82063669.
E-mail address: mustafa.aghazadeh@gmail.com (M. Aghazadeh).

0272-8842/$ - see front matter © 2013 Elsevier Ltd and Techna Group S.r.l. All rights reserved.
http://dx.doi.org/10.1016/j.ceramint.2013.05.067

It has been also reported that $La(OH)_3$ nanorod arrays can be grown on Cu substrate by cathodic deposition in a solution of 0.01 mol L^{-1} $La(NO_3)_3$+0.01 mol L^{-1} NH_4NO_3 under galvanostatic conditions by applying I_a of 0.75 mA cm^{-2} at bath temperature of 70 °C [27]. Recently, we performed pulse cathodic electrodeposition of $La(OH)_3$ from nitrate bath for the first time [28], and vertically-aligned nanorods of $La(OH)_3$ were prepared at the applied conditions, *i.e.* t_{on}=5 s and t_{off}=10 s, and I_a=1 mA cm^{-2}. It was also found that heat-treatment of the prepared $La(OH)_3$ nanorods results the La_2O_3 nanorods without any change in their morphology [28]. Lui et al. have demonstrated that $La(OH)_3$ nanospindles and nanorods can be obtained by galvanostatic deposition (I=1 mA cm^{-2}) on F-doped SnO_2 substrates from 0.01 M La $(NO_3)_3$+50 vol% DMSO bath at temperature of 70 °C [29]. They observed that morphology of the deposits can be easily tuned by adjusting the concentration of DMSO. It was reported that capsule-like nanostructures of $La(OH)_3$ can be easily prepared *via* cathodic electrodeposition from nitrate bath at low temperature of 10 °C and the current density of 1 mA cm^{-2} [31]. Heat-treatment of the $La(OH)_3$ nanocapsules has resulted the La_2O_3 nanoplates [32]. Bocchetta et al. reported that the high quality arrays of $Ln(OH)_3$ (Ln=La and Nd) nanowires can be prepared by cathodic electrodeposition from nitrate bath using anodic alumina membrane as a template at the experimental conditions of i=1 mA cm^{-2} in 0.05 M Ln $(NO_3)_3$ [30]. In this work, we tuned simple electrochemical conditions for the preparation of La_2O_3 nanowires at large scale without using any template and additive. In fact, we found that nanowires of $La(OH)_3$ can be easily deposited on the steel substrate from an aqueous solution of 0.005 M La $(NO_3)_3$ by only applying the current density of 2 mA cm^{-2} at RT condition. Heat treatment of the hydroxide nanowires at 600 °C for 3 h is also resulted the La_2O_3 nanowires. This work provides a simple electrochemical route for the preparation of $La(OH)_3$ and La_2O_3 nanowires on a large scale.

2. Experimental procedure

2.1. Chemicals

$La(NO_3)_3$•$6H_2O$ (Merck) was used as received. All solutions were prepared using double distilled water. Aqueous solution of 5 mM $La(NO_3)_3$•$6H_2O$ was prepared for electrodeposition.

2.2. Sample preparation

The electrochemical set up was a simple two electrode system including a stainless steel cathode (316L, 100 mm × 50 mm × 0.5 mm) centered between the two parallel graphite counter electrodes. The deposition experiments were performed at a current density of 2 mA cm^{-2} for 30 min. After deposition, the steel substrates were rinsed with water several times, and dried at room temperature for 10 h. The deposits were then scraped from the substrates and subjected to further analyses. To obtain oxide product, the hydroxide powder was heat treated at 600 °C for 3 h in dry air atmosphere.

2.3. Characterization

XRD patterns of the products were recorded using a Phillips PW-1800 diffractometer with Cu Kα radiation (λ=1.5406 Å) at a scanning rate of 1°/min. Chemical bonding information on metal–oxygen, metal–anions, and hydroxyl were studied with Fourier transform infrared spectroscopy (FTIR, Bruker Vector 22) using a potassium bromide (KBr) pellet technique. Each FTIR spectrum was collected after 20 scans at a resolution of 4 cm^{-1} from 400 to 4000 cm^{-1}. Carbon, nitrogen, and hydrogen contents of the hydroxide powder were determined by CHN analysis using Elementar Vario ELIII analyzer. Thermogravimetric analysis (DSC–TGA) was carried out in air between room temperature and 600 °C at a heating rate of 5 °C min^{-1} using a thermoanalyzer (STA-1500). The surface morphologies were observed using a scanning electron microscope (SEM, LEO 1455 VP, Oxford, UK, operating voltage 15 kV) by mounting a small amount of the prepared products on a conducting carbon tape and sputter coating with Pt to improve the conductivity.

3. Results and discussion

3.1. Deposit formation mechanism

In the electrochemical deposition, controlling the rates of processes such as electrochemical reactions, and nucleation and growth of deposit through experimental parameters such as current density, potential, bath temperature, and reaction medium are key factors in designing new products with desired crystallinity and morphology [45,49–53]. It was reported that the important aspect in the cathodic electrodeposition of metal hydroxides is the reduction of an oxygen precursor on the cathode, which results the base production at its surface [51–54]. This would control the nucleation and the growth rates, and significantly affects the structural and morphological characteristics of the obtained hydroxide deposit. The formation of $La(OH)_3$ deposit on the cathode can be explained by the following steps, as schematically shown in Fig. 1 [28–32]:

– Electrochemical step:

$$2H_2O+2e^- \rightarrow H_2+2OH^- \quad E^\circ=-1.08 \text{ V } vs. \text{ Ag/AgCl} \quad (1)$$

– Chemical step:

$$La^{3+}(aq)+3OH^-(aq)+yH_2O \rightarrow [La(OH)_3 \cdot yH_2O]\downarrow \quad (2)$$

$$La^{3+}(aq)+3OH^-(aq)+xNO_3^-+yH_2O \rightarrow [La(OH)_{(3-x)}(NO_3)_x \cdot yH_2O]\downarrow \quad (3)$$

Fig. 1a shows the potential value during the electrodeposition of $La(OH)_3$ form nitrate bath at current density of 2 mA cm^{-2}. The recorded potential value (−1.19 V *vs.* Ag/AgCl, as seen in Fig. 1a) revealed that the reduction of water (Eq. (1)) has the major role in the base electrogeneration at our experimental conditions. Notably, the strings of gas

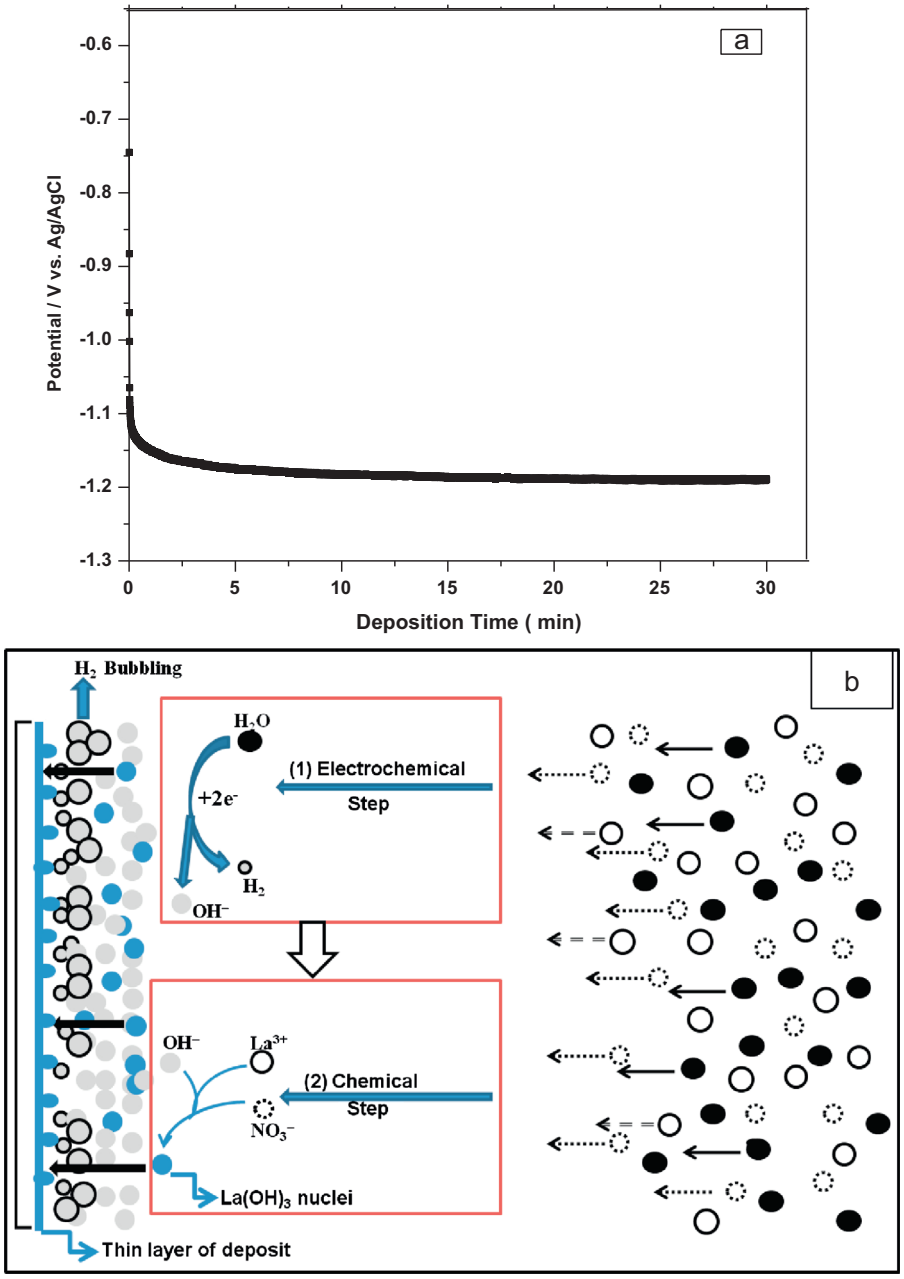

Fig. 1. (a) Potential–time curve for $La(OH)_3$ deposition on the steel cathode from nitrate bath at I_a of 2 mA cm^{-2} and (b) schematic view of the deposition formation.

bubbles are experimentally observed on the cathode surface in all times of deposition, which clearly confirmed the base electrogeneration *via* water reduction. So, the electrochemical step includes water reduction on the cathode surface, and production of OH^- ions and H_2 gas (as schematically shown in Fig. 1b). This step results an increase of local pH at the cathode surface. By reaching the pH values to the $La(OH)_3$ deposition conditions, the chemical step is started and lanthanum hydroxide is sequentially formed and deposited on the cathode surface (as schematically shown in Fig. 1b). Considering the solubility constant of $La(OH)_3$ ($K_{sp}=[La^{3+}][OH^-]^3=1\times10^{-19}$ at 25 °C [55]), it is expected that the OH^- ions produced in the electrochemical step being to consume in the chemical step at pH of 7.5.

The potential value of cathode (−1.19 V *vs.* Ag/AgCl, Fig. 1a) during the electrodeposition is also disclosed that nitrate ions have no role in the base electrogeneration. However, they can intercalate in the hydroxide structure and deposit on the cathode surface, *i.e.* they can contribute in the chemical step (as schematically shown in Fig. 1b). To confirm this matter, the obtained deposit was analyzed by CHN analysis and the results showed the 0.23% C, 2.99% H and 0.85% N in the hydroxide composition. The existence of nitrogen in the deposit composition reveals that the nitrate ions have intercalated in the chemical step. In fact, the chemical step has taken place *via* the reaction (3), as schematically shown in Fig. 1b. The existence of carbon and hydrogen discloses the presence of carbonate ions (originating from

adsorbed air-CO_2 by sample during the analysis), and presence of the physically and the chemically bounded water molecules in the deposit structure, respectively. Thus, the formula of [La $(OH)_{(3-x)}$ $(NO_3)_x \cdot yH_2O$] is proposed for the electrodeposited hydroxide, where x and y are the amount of nitrate ions and water molecules incorporated in the hydroxide structure, respectively. To determine the values of x and y, and also investigation of physico-chemical changes during the heat-treatment, thermal behavior of the hydroxide sample was analyzed by DSC–TGA.

3.2. Oxide formation mechanism

To obtain the oxide product, the prepared deposit was heat treated at 600 °C for 3 h. The physico-chemical changes during the calcination were investigated by DSC–TG analysis. The results of DSC–TG (thermal behavior) of the hydroxide powder are shown in Fig. 2. In the DSC curve, four endothermic peaks can be seen (i–iv), which are corresponded to the following changes:

(i) Removal of the physically adsorbed water below 200 °C:

$$[La(OH)_{(3-x)}(NO_3)_x \cdot yH_2O] \rightarrow [La(OH)_{(3-x)}(NO_3)_x] + yH_2O \quad (4)$$

(ii) Removal of the structural water between 200 and 380 °C:

$$[La(OH)_{(3-x)}(NO_3)_x] \rightarrow [LaO(OH)_{(1-x)}(NO_3)_x] + (2-x)H_2O \quad (5)$$

(iii) Removal of the residual structural water between 380 and 475 °C:

$$[LaO(OH)_{(1-x)}(NO_3)_x] \rightarrow 2LaO(NO_3)_x + (1-x)H_2O, \text{ and} \quad (6)$$

(iv) Removal of the intercalated nitrate ions at 475 and 600 °C:

$$LaO(NO_3)_x \rightarrow La_2O_3 + 2xNO_2 + x/2O_2 \quad (7)$$

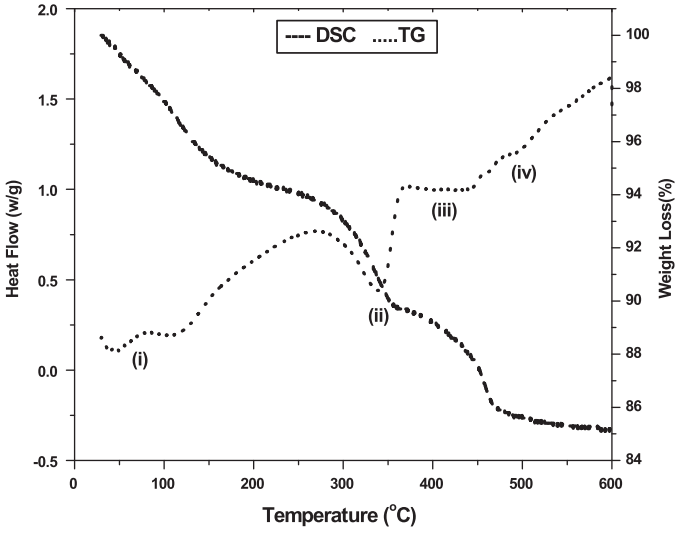

Fig. 2. DSC–TG curves of the $La(OH)_3$ sample.

Total weight loss of the hydroxide sample is 14.9 wt%. Approximately 4.5 wt% of the total weight loss corresponds to the physically adsorbed water (Eq. (4)). The weight losses of ~6 wt% is also corresponded to the elimination of the structural water (Eq. (5)) and ~3.1 wt% of total weight loss is also related to the removal of the residual structural water (Eq. (6)), which are relatively lower than the theoretical values (9.5 and 4.5 mass% respectively). This can be related to the intercalated nitrate ions, which reduced the amount of the structural water of the hydroxide sample. Finally, the last weight loss (1.3 wt%) is corresponded to the removal of intercalated nitrate ions (Eq. (7)). These results are in agreement with the reported data in literature [16–18].

3.3. Characterization

3.3.1. XRD

The XRD patterns of the hydroxide precursor and the oxide product are shown in Fig. 3. All diffraction peaks in the hydroxide pattern (Fig. 3a) can be assigned as the hexagonal phase of La $(OH)_3$ with the lattice constants of $a=6.528$ Å and $c=3.858$ Å, which are consistent with the standard card (JCPDS 41-4019). Notably, some irregularities are observed in the peak positions and their intensities (Fig. 3a), which discloses that the hydroxide sample has not been completely crystallized. This may be originated from the existence of the intercalated nitrate ions and the physically adsorbed water in the structure of deposited sample. Also, all of the diffraction peaks in the XRD pattern of hydroxide sample (Fig. 3a) are broad. In general, peak broadening in the XRD pattern is related to (i) crystallite size effects and (ii) increased degree of disordering on account of the existence of structural defects, such as stacking faults/growth faults and proton vacancies, or the adsorption of inorganic species like as water molecules and different anions. Hence, broadening of the diffraction peaks in XRD pattern of hydroxide sample can be related to the adsorption of water molecules and nitrate anions in the hydroxide structure. Notably, the existence of these species in the hydroxide structure was confirmed by CHN and IR analyses. The XRD pattern of the heat treated sample is shown in Fig. 3b. All of the diffraction peaks observed in the oxide pattern (Fig. 3b) are easily indexed to a pure hexagonal phase of La_2O_3 (JCPDS 05-0602) with lattice constants $a=3.397$ Å and $c=6.129$ Å. The peaks are well-defined and sharp, and no additional peaks from any impurities are found, indicating the obtained La_2O_3 powder is well-crystallized with high purity. The XRD results confirmed the formation of crystalline oxide product from the heat treatment of the electrodeposited hydroxide precursor, and are in agreement with DSC–TG results.

3.3.2. FT-IR

Fig. 4 displays the FT-IR spectra of the hydroxide precursor and the oxide product. IR spectrum of the hydroxide sample (Fig. 4a) has the typical peaks of the physically adsorbed H_2O and the structural O–H of $La(OH)_3$. An intense and sharp band at 3605 cm^{-1} is assigned to the stretching and bending O–H vibrations of lanthanum hydroxide [20–23]. The bands at 3430 cm^{-1}, 1640 cm^{-1} and 672 cm^{-1} are associated with the hydroxyl groups of molecular H_2O (at both samples). A sharp peak at 1383 cm^{-1} in

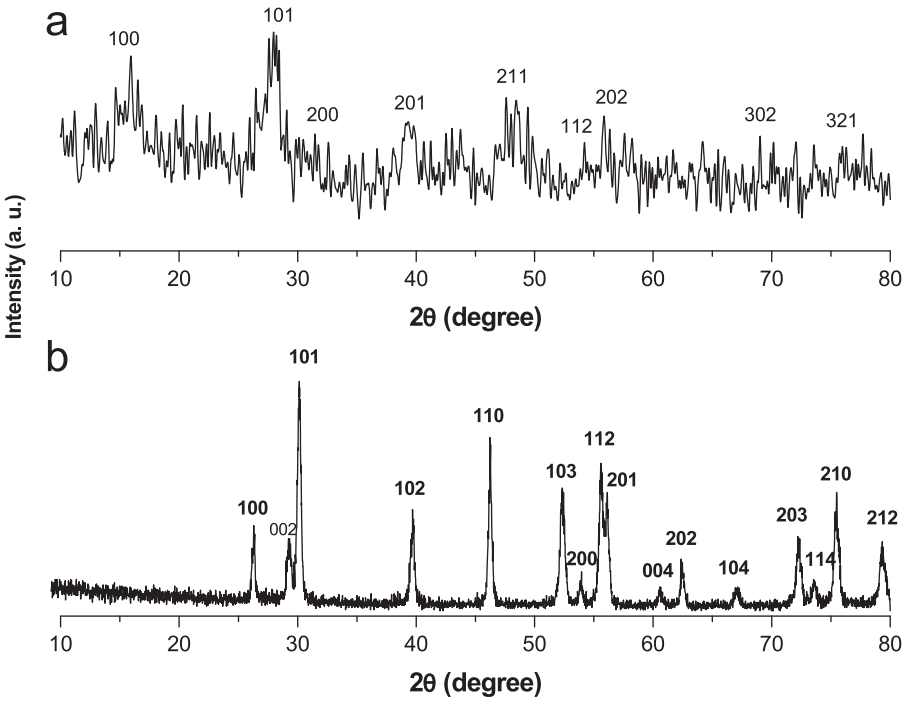

Fig. 3. XRD patterns of (a) the electrodeposited hydroxide sample and (b) the oxide product obtained after the heat-treatment at 600 °C for 3 h.

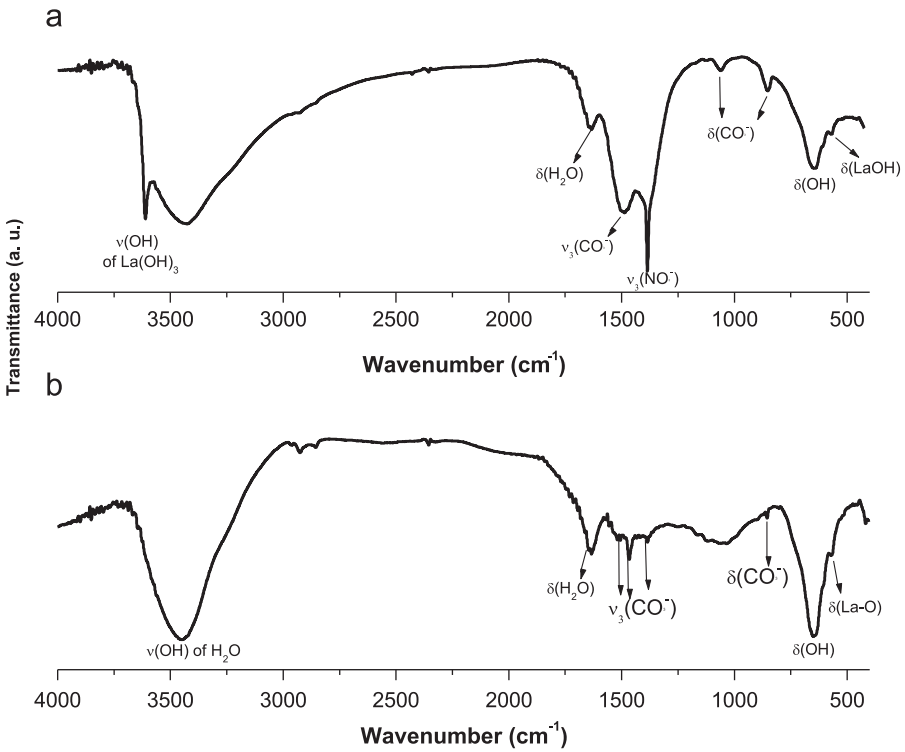

Fig. 4. IR spectra of (a) $La(OH)_3$ and (b) La_2O_3 nanowires.

the hydroxide spectra (Fig. 4a) is assigned to the vibration modes of NO_3^- anions intercalated in the deposit structure during the chemical step (Eq. (3)), which is in agreement with the DSC–TGA results and also confirmed the proposed mechanism. Notably, no band at 1383 cm^{-1} is observed in the spectra of the oxide sample (Fig. 4b), which disclosed that the nitrate ions are removed during the heat-treatment (as confirmed by the DSC–TG analysis). In both spectra (Fig. 4a and b), the peaks at about 1540 cm^{-1}, 1035 cm^{-1} and 825 cm^{-1} are attributed to the carbonate group, which originate from the reaction of samples with air-CO_2 during the analysis, which is in agreement with CHN results. The two distinct bands at 445 cm^{-1} (in Fig. 4a) and 505 cm^{-1} (in Fig. 4b) are

characteristic of the La–OH and La–O–La bond vibrations in La $(OH)_3$ and La_2O_3, respectively [24–26].

3.3.3. SEM

Morphological characteristics of the hydroxide precursor and the oxide product are shown in Fig. 5. For the hydroxide sample (Fig. 5a and b), the wire-like morphology at nanoscale is clearly seen. The hydroxide wires have no specific growth direction and also are rather agglomerated or stacked together (Fig. 5b). The hydroxide wires are approximately 50 nm in diameter and have length up to 400 nm. After the heat-treatment, it can be seen that morphology of the wires has no significant change and their primary shape and agglomerated nature have been preserved during the heat-treatment, as seen in Fig. 5c and d. However, the size of the oxide wires has been rather enlarged as one can seen from Fig. 5a and c. In fact, size of the oxide wires has been rather enlarged as compared with their precursor, *i.e.*, hydroxide wires. The oxide wires have diameter of approximately 100 nm and length up to 500 nm. These changes in the size of oxide wires can be explained in the term of aggregation of the hydroxide wires during the heat-treatment. It is possible that the stacked or agglomerated hydroxide wires are connected to each other on heating, which results the larger oxide wires. Notably, we previously found that the heat-treatment of the $La(OH)_3$ nanocapsules has a significant effect on their morphologies and leads to the formation of La_2O_3 nanoplates [32], where, we found that the capsule-like particles have high tendencies to interconnect with each other on heating, which produce larger plate-like oxide particles. Recently, Wu et al. found that the $La(OH)_3$ nanorods, prepared by the solvothermal route, transformed to the La_2O_3 nanoplates during heating [25]. However, in most cases, La_2O_3 nanorods have been reported as the product of heat treatment of $La(OH)_3$ nanorods [18,23–26,28,29,33]. Based on these reports, it can be said that the same process occurred on the structure of hydroxide wires during the heat-treatment as a result of the removal of water molecules and intercalated ions. These changes can cause to interconnection of the hydroxide wires (especially stacked ones) to each other and so formation of larger oxide wires (Fig. 5c and d). $La(OH)_3$ and La_2O_3 nanowires could be beneficial to the catalytic, superconductive, hydrogen storage, piezo-electricity, thermoelectricity and sorbent capability. They can be also used as the template for the synthesis of nanostructures of other materials.

4. Conclusion

La_2O_3 nanowires were prepared by a simple and facile two-step synthetic route. First, hydroxide precursor was directly electrodeposited on the steel substrate from an additive-free lanthanum nitrate bath at a current density of 2 mA cm^{-2}. The obtained deposit was then heat treated at 600 °C for 3 h. Morphological characterization by SEM, and structural analysis *via* XRD and IR revealed that uniform La_2O_3 nanowires at large scale can be prepared by this simple method. In final, mechanism of the deposit formation during the electrodeposition process, and physico-chemical changes of the hydroxide precursor during the heat-treatment were proposed and discussed.

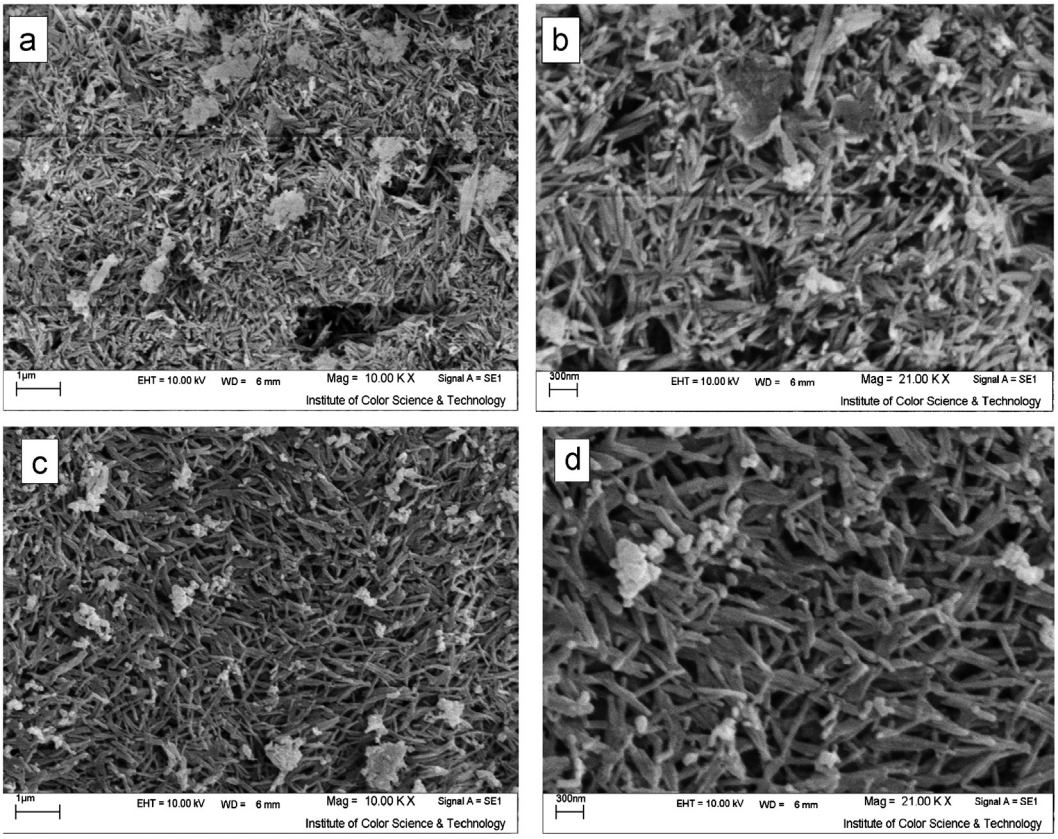

Fig. 5. SEM images of (a,b) $La(OH)_3$ and (c,d) La_2O_3 nanowires.

References

[1] P.C. Chen, C.H. Chen, C.M. Tsai, C.F. Cheng, S.L. Wu, Nitride-based metal–insulator–semiconductor ultraviolet sensors with a sputtered lanthanum oxide (La_2O_3) insulator, Surface and Coatings Technology (2013) in press.

[2] B. Ersoy, V. Gunay, Effects of La_2O_3 addition on the thermal stability of γ-Al_2O_3 gels, Ceramics International 30 (2004) 163–170.

[3] W. He, S. Schuetz, R. Solanki, J. Belot, J.M. Andrew, Atomic layer deposition of lanthanum oxide films for high-κ gate dielectrics, Electrochemical Solid-State Letter 7 (2004) G131–G133.

[4] W. Chen, Z. Kang, B. Ding, Nanostructured W–La_2O_3 electrode materials with high content La_2O_3 doping, Materials Letters 59 (2005) 1138–1141.

[5] M. Mori, Y. Hiei, T. Yamamoto, H. Itoh, Lanthanum alkaline earth manganites as a cathode material in high-temperature solid oxide fuel cells, Journal of the Electrochemical Society 146 (1999) 4041–4047.

[6] J. Yoo, J. Hong, H. Lee, Y. Jeong, B. Lee, H. Song, J. Kwon, Piezoelectric and dielectric properties of La_2O_3 added Bi(Na, K)TiO_3–$SrTiO_3$ ceramics for pressure sensor application, Sensors and Actuators A: Physical 126 (2006) 41–47.

[7] U. Rambabu, Sang-Do Han, Synthesis and luminescence properties of broad band greenish-yellow emitting $LnVO_4$:Bi^{3+} and (Ln_1, Ln_2)VO_4:Bi^{3+} (Ln = La, Gd and Y) as down conversion phosphors, Ceramics International 39 (2013) 701–708.

[8] S. Long, J. Hou, G. Zhang, F. Huang, Y. Zeng, High quantum efficiency red-emission tungstate based phosphor $Sr(La_{1-x}Eu_x)_2Mg_2W_2O_{12}$ for WLEDs application, Ceramics International 39 (2013) 6013–6017.

[9] Z. Lu, T. Wanjun, Synthesis and luminescence properties of Eu^{3+}-activated $NaLa(MoO_4)(WO_4)$ phosphor, Ceramics International 38 (2012) 837–840.

[10] X. Liu, L. Yan, J. Zou, Tunable cathodoluminescence properties of Tb^{3+}-doped La_2O_3 nanocrystalline phosphors, Journal of the Electrochemical Society 157 (2010) P1–P6.

[11] G. Mao, H. Zhang, H. Li, J. Jin, S. Niu, Selective synthesis of morphology and species controlled La_2O_3:Eu^{3+} and $La_2O_2CO_3$:Eu^{3+} phosphors by hydrothermal method, Journal of the Electrochemical Society 159 (2012) J48–J53.

[12] D. Zhang, S. Shi, M. Luo, J. Zhou, Solid state reaction preparation and enhanced red luminescence of S-doped $La_2Mo_2O_9$:Pr^{3+} phosphors, Ceramics International (2013) in press.

[13] D. Andriamasinoro, R. Kieffer, A. Kiennemann, P. Poix, Preparation of stabilized copper-rare earth oxide catalysts for the synthesis of methanol from syngas, Applied Catalysis 106A (1993) 201–212.

[14] Y. Cui, H. Zhang, H. Xu, W. Li, The CO_2 reforming of CH_4 over Ni/La_2O_3/α-Al_2O_3 catalysts: the effect of La_2O_3 contents on the kinetic performance, Applied Catalysis A 331 (2007) 60–69.

[15] K.O. Rocha, J.B.O. Santos, D. Meira, P.S. Pizani, C.M.P. Marques, D. Zanchet, J.M.C. Bueno, Catalytic partial oxidation and steam reforming of methane on La_2O_3–Al_2O_3 supported Pt catalysts as observed by X-ray absorption spectroscopy, Applied Catalysis A: General 431 (2012) 79–87.

[16] L.G. Rovira, J.M. Sanchez-Amaya, M. Lopez-Haro, A.B. Hungria, Z. Boukha, S. Bernal, F.J. Botana, Formation and characterization of nanotubes of $La(OH)_3$ obtained using porous alumina membranes, Nanotechnology 19 (2008) 495305–495309.

[17] D. Zheng, J. Shi, X. Lu, C. Wang, Controllable growth of $La(OH)_3$ nanorod and nanotube arrays, Crystal Engineering Communication 10 (2010) 4066–4070.

[18] B. Tang, J. Ge, C. Wu, L. Zhuo, J. Niu, Z. Chen, Z. Shi, Y. Dong, Sol–solvothermal synthesis and microwave evolution of $La(OH)_3$ nanorods to La_2O_3 nanorods, Nanotechnology 15 (2004) 1273–1276.

[19] J. Zhu, Z. Gui, Y. Ding, A simple route to lanthanum hydroxide nanorods, Materials Letters 62 (2008) 2373–2376.

[20] J. Deng, L. Zhang, C.T. Au, H. Dai, Template-free synthesis of high surface area single crystalline lanthanum hydroxide nanorods *via* a low-temperature solution route, Materials Letters 63 (2009) 632–634.

[21] L. Qian, Y. Gui, S. Guo, Q. Gong, X. Qian, Controlled synthesis of light rare-earth hydroxide nanorods *via* a simple solution route, Journal of Physics and Chemistry of Solids 70 (2009) 688–693.

[22] X. Ma, H. Zhang, J. Xu, D. Yang, Synthesis of ultrafine lanthanum hydroxide nanorods by a simple hydrothermal process, Materials Letters 58 (2004) 1180–1182.

[23] Q. Mu, Y. Wang, Synthesis, characterization, shape-preserved transformation, and optical properties of $La(OH)_3$, $La_2O_2CO_3$, and La_2O_3 nanorods, Journal of Alloys and Compounds 509 (2011) 396–401.

[24] J. Ding, Y. Wu, W. Sun, Y. Li, Preparation of $La(OH)_3$ and La_2O_3 with rod morphology by simple hydration of La_2O_3, Journal of Rare Earths 24 (2006) 440–442.

[25] Y. Wu, Y. Chen, J. Zhou, $La(OH)_3$ nanorods and La_2O_3 nanoplates: facile synthesis and photoluminescence properties, Materials Letters 95 (2013) 5–8.

[26] N. Zhang, R. Yi, L. Zhou, G. Gao, R. Shi, G. Qiu, X. Liu, Lanthanide hydroxide nanorods and their thermal decomposition to lanthanide oxide nanorods, Materials Chemistry and Physics 114 (2009) 160–167.

[27] C.Z. Yao, B.H. Weia, H.X. Ma, Q.J. Gong, K.W. Jing, H. Sun, L. X. Meng, Facile fabrication of $La(OH)_3$ nanorod arrays and their application in wastewater treatment, Materials Letters 65 (2011) 490–492.

[28] F. Khosrow-pour, M. Aghazadeh, B. Arhami, Facile synthesis of vertically aligned one-dimensional (1D) $La(OH)_3$ and La_2O_3 nanorods by pulse current deposition, Journal of the Electrochemical Society 160 (2013) D150–D155.

[29] Z. Liu, D. Zheng, Y. Su, Z. Liu, Y. Tong, Facile and efficient electrochemical synthesis of lanthanum hydroxide nanospindles and nanorods, Electrochemical and Solid-State Letters 13 (2010) E15–E18.

[30] P. Bocchetta, M. Santamaria, F.D. Quarto, Template electrosynthesis of $La(OH)_3$ and $Nd(OH)_3$ nanowires using porous anodic alumina membranes, Electrochemistry Communications 9 (2007) 683–688.

[31] M. Aghazadeh, A. Nozad Golikand, M. Ghaemi, T. Yousefi, A novel lanthanum hydroxide nanostructure prepared by cathodic electrodeposition, Materials Letters 65 (2011) 1466–1468.

[32] M. Aghazadeh, A. Nozad Golikand, M. Ghaemi, T. Yousefi, La_2O_3 nanoplates prepared by heat-treatment of electrochemically grown $La(OH)_3$ nanocapsules from nitrate medium, Journal of the Electrochemical Society 158 (2011) E136–E141.

[33] B. Tang, J. Ge, L. Zhuo, The fabrication of $La(OH)_3$ nanospheres by a controllable hydrothermal method with citric acid as a protective agent, Nanotechnology 15 (2004) 1749–1751.

[34] C. Hu, H. Liu, W. Dong, Y. Zhang, G. Bao, C. Lao, Z.L. Wang, $La(OH)_3$ and La_2O_3 Nanobelts—synthesis and physical properties, Advanced Materials 19 (2007) 470–474.

[35] M. Nieminen, M. Putkonen, L. Niinisto, Formation and stability of lanthanum oxide thin films deposited from β-diketonate precursor, Applied Surface Science 174 (2001) 155–165.

[36] B.Y. Kim, M.G. Ko, E.J. Lee, M.S. Hong, Y.J. Jeon, J.W. Park, Atomic layer deposition of La_2O_3 thin films by using an electron cyclotron resonance plasma source, Journal of the Korean Physical Society 49 (2006) 1303–1306.

[37] C. Yang, H. Fan, S. Qiu, Y. Xi, Y. Fu, Microstructure and dielectric properties of La_2O_3 films prepared by ion beam assistant electron-beam evaporation, Journal of Non-Crystalline Solids 355 (2009) 33–37.

[38] C. Sun, G. Xiao, H. Li, L. Chen, Mesoscale organization of flower-like $La_2O_2CO_3$ and La_2O_3 microspheres, Journal of the American Ceramic Society 90 (2007) 2576–2581.

[39] J. Sheng, S. Zhang, S. Lv, W. Sun, Surfactant-assisted synthesis and characterization of lanthanum oxide nanostructures, Journal of Material Science 42 (2007) 9565–9571.

[40] T. Masui, Y. Kato, Preparation of the cubic-type La_2O_3 phase by thermal decomposition of LaI_3, Journal of Solid State Chemistry 178 (2005) 395–398.

[41] X. Wang, M. Wang, H. Song, B. Ding, A simple sol–gel technique for preparing lanthanum oxide nanopowders, Materials Letters 60 (2006) 2261–2265.

[42] D. Stoychev, I. Valov, P. Stefanov, G. Atanasova, M. Stoycheva, Ts. Marinova, Electrochemical growth of thin La_2O_3 films on oxide and metal surfaces, Materials Science and Engineering C 23 (2003) 123–128.

[43] I. Zhitomirsky, L. Gal-Or, Characterization of zirconium, lanthanum and lead oxide deposits prepared by cathodic electrosynthesis, Journal of Materials Science 33 (1998) 699–705.

[44] Y. Wang, L. Yang, Y. Wang, X. Wang, L. Wang, Facile electrochemical synthesis of $PbWO_4$ dendrites, Ceramics International (2013) in press.

[45] M. Aghazadeh, M. Hosseinifard, Electrochemical preparation of ZrO_2 nanopowder: impact of the pulse current on the crystal structure, composition and morphology, Ceramics International 39 (2013) 4427–4435.
[46] M. Aghazadeh, A.A. Malek Barmi, H. Mohammad Shiri, S. Sedaghat, Cathodic electrodeposition of $Y(OH)_3$ and Y_2O_3 nanostructures from chloride bath. Part II: effect of the bath temperature on the crystal structure, composition and morphology, Ceramics International 39 (2013) 1045–1055.
[47] F. Jamali-Sheini, R. Yousefi, Electrochemical synthesis and surface characterization of hexagonal Cu–ZnO nano-funnel tube films, Ceramics International 39 (2013) 3715–3720.
[48] C.Y. Chen, S.C. Wang, C.Y. Lin, F.S. Chen, C.K. Lin, Electrophoretically deposited manganese oxide coatings for supercapacitor application, Ceramics International 35 (2009) 3469–3474.
[49] Y. Xua, Y. Chen, J. Wu, D. Li, H. Ju, J. Zheng, The determination of the kinetic parameters of electrochemical reaction in chemical power sources: a critical review, International Journal of Hydrogen Energy 35 (2010) 6366–6380.
[50] W.J. Zhou, D.D. Zhao, M.W. Xu, C.L. Xu, H.L. Li, Effects of the electrodeposition potential and temperature on the electrochemical capacitance behavior of ordered mesoporous cobalt hydroxide films, Electrochimica Acta 53 (2008) 7210–7219.
[51] M. Aghazadeh, Cathodic electrodeposition of ZrO_2: impact of current density on the crystal structure, composition and morphology, Journal of the Electrochemical Society 159 (2012) E53–E58.
[52] B. Liu, X.Y. Wang, H.T. Yung, Y.S. Zhang, D.Y. Song, Z.X. Zhou, Physical and electrochemical characteristics of aluminium-substituted nickel hydroxide, Journal of Applied Electrochemistry 29 (1999) 855–860.
[53] D. Zhao, W. Zhou, Effects of deposition potential and anneal temperature on the hexagonal nanoporous nickel hydroxide films, Chemistry of Materials 19 (2007) 3882–3891.
[54] I. Zhitomirsky, Cathodic electrodeposition of ceramic and organoceramic materials: fundamental aspects, Advanced Colloid Interface Science 97 (2002) 279–317.
[55] C.F. Baes, R.E. Mesmer, Hydrolysis of Cations, Wiley, New York, 1976.